Turbulent transition of thermocapillary flow induced by water evaporation

C. A. Ward* and Fei Duan
Thermodynamics and Kinetics Laboratory, Department of Mechanical and Industrial Engineering, University of Toronto, 5 King's College Road, Toronto, Canada M5S 3G8
(Received 28 February 2003; published 25 May 2004)

Water has been examined for thermocapillary convection while maintained just outside the mouth of a stainless-steel, conical funnel where it evaporated at different but steady rates. Evaporation at a series of controlled rates was produced by reducing the pressure in the vapor-phase to different but constant values while maintaining the temperature of the water a few millimeters below the interface at 3.56 ± 0.03 °C in each case. Since water has its maximum density at 4 °C, these conditions ensured there would be no buoyancy-driven convection. The measured temperature profile along the liquid-vapor interface was found to be approximately axisymmetric and parabolic with its minimum on the center line and maximum at the periphery. The thermocapillary flow rate was determined in two ways: (1) It was calculated from the interfacial temperature gradient measured along the interface. (2) The deflection of a 12.7-μm-diameter, cantilevered probe inserted into the flow was measured and the liquid velocity required to give that deflection determined. The values determined by the two methods agree reasonably. As the vapor-phase pressure was reduced, the thermocapillary flow rate increased until a limiting value was reached. When the pressure was reduced further, certain of the variable relations underwent a bifurcation and the power spectrum of the probe displacement indicated it was a periodic function with frequency locking. These results suggest that thermocapillary flow plays an important role in the energy transport near the interface of evaporating water. In particular, it appears that the subinterface, uniform-temperature layer, reported in earlier studies, results from the mixing produced by the thermocapillary flow. The Stefan boundary condition is often applied to determine the energy flux to an interface where phase change is occurring; however, when there is strong convective flow parallel to the interface, the normal Stefan condition does not give an adequate description of the energy transport.

DOI: 10.1103/PhysRevE.69.056308 PACS number(s): 47.27.Cn

I. INTRODUCTION

Thermocapillary (or Marangoni) convection in many liquids has been observed [1], but for pure water its existence has been contentious. Barnes and Hunter [2] have reported water evaporation experiments in which the Marangoni number was much greater than the critical value [3,4], and thus, thermocapillary convection should have been present but its effects were not observed. Cammenga *et al.* [5] have pointed out the absence of experimental evidence supporting the existence of thermocapillary convection for water, and in recent studies of another substance (SF6) Garrabos *et al.* [6] reported that even though a temperature gradient along an interface was thought to be present no thermocapillary convection was observed. The mechanism by which a temperature gradient can exists along a liquid-vapor interface without producing thermocapillary convection has not been established, although it is usually assumed that impurities accumulating at the interface of water are responsible (e.g., Ref. [7]). But this mechanism has not been experimentally established, and careful experiments [5] with pure water have been conducted in which it is hard to imagine that impurities could be responsible for the absence of thermocapillary convection.

We note that evidence supporting the absence of thermocapillary convection for water has been indirect, in the sense that the temperature along a liquid-vapor interface was not directly measured [2,5–7]. Our hypothesis is that thermocapillary convection occurs in water if there is a temperature gradient along the liquid-vapor interface. To explain the previous observations that did not observe thermocapillary convection of water when it was expected, our hypothesis suggests that the temperature field at the liquid-vapor interface during water evaporation was different than that assumed.

In support of our hypothesis, we note that earlier studies of water evaporation [8–12] provided indirect evidence of thermocapillary convection, and indicated a temperature discontinuity at the liquid-vapor interface in which the interfacial temperature in the vapor was greater than that in the liquid phase by as much as 7.8 °C. This temperature discontinuity was not considered by any of the previous investigators, to our knowledge.

In previous experiments, the temperature profile on the center line of evaporating water indicated the presence of "mixing" near the interface. The circumstance under which the previous measurements were made is indicated schematically in Fig. 1(a) [12]. The water-vapor interface was maintained just outside the mouth of a conical funnel. Water was pumped in the bottom of the funnel at the same rate as the water evaporated. The temperature at the funnel throat was maintained constant. The measured center line temperature immediately below the interface in the liquid phase as a function of depth was approximately uniform. The maximum depth of the uniform-temperature layer was ~0.5 mm. Below the uniform-temperature layer, the temperature-depth

*Corresponding author. Fax: 416-978-7322. Email address: ward@mie.utoronto.ca

 ©2004 The American Physical Society

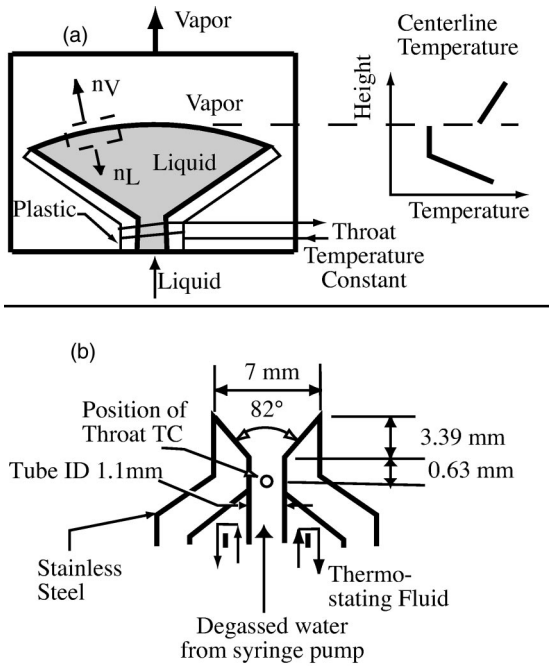

FIG. 1. (a) A schematic of the experimental apparatus used to measure the uniform-temperature layer is shown [12], along with a sketch of the temperature profile measured on the centreline. Note the uniform-temperature layer immediately below the interface and the temperature discontinuity at the phase boundary. (b) Schematic of the stainless-steel funnel used in the present experiments.

profile indicated thermal conduction from the funnel throat to the bottom of the uniform-temperature layer, but the mechanism of energy transport across the uniform-temperature layer to the interface (where the phase change process was occurring) was unclear. One mechanism that has to be considered is thermocapillary convection.

To investigate this mechanism, a funnel and cooling system, indicated schematically in Fig. 1(b), have been devised. In the experiments reported herein, the maximum temperature of the water in the funnel was at the funnel throat and was less than 4 °C—the temperature at which water has its maximum density. The water at the funnel mouth was evaporated at a steady rate by controlling the vapor-phase pressure. This evaporation cooled the water at the funnel mouth to temperatures well below the temperature at the funnel throat. Since the density of water decreases with decreasing temperature for temperatures below 4 °C the lightest liquid was at the top of the funnel; thus, there would have been no potential for the buoyancy-driven convection. Any observed effects of convection in these experiments could only come from thermocapillary convection.

A necessary condition for thermocapillary convection to be present is that a temperature gradient exists parallel to the water-vapor interface. In the previous experiments, the temperature as a function of depth was measured only on the center line [8–12]. In the modified apparatus, the temperature profile parallel to a spherical (pure) water-vapor interface can be measured as the water evaporates under steady-state conditions while maintained at the circular mouth of a stainless-steel funnel [Fig. 1(b)]. The temperature measurements indicate an axisymmetric, parabolic temperature profile along the interface with the minimum on the funnel center line and maximum at the periphery (see below). Thus, the Marangoni effect would induce fluid motion from the periphery toward the center line.

Two methods for determining the fluid speed parallel to the interface have been investigated. In one, the measured temperature gradient parallel to the surface is used to calculate the fluid speed, and in the other a 12.7-μm-diameter, metal cylinder mounted as a vertical, cantilever beam (52 mm in length) was inserted 40 μm into the liquid phase while the water evaporated steadily. By measuring the deflection of the cylinder tip, the mean fluid speed could also be inferred. In a series of evaporation experiments, the values of the fluid speed determined by the two methods are found to agree (surprisingly) well. These results strongly support the existence of thermocapillary flow for pure water.

Also, the measured temperature profiles in the liquid and vapor-phases allow the heat conducted to the interface from each bulk phase to be determined. Both of these modes of energy transport are accounted for in the Stefan condition [13,14] but this condition neglects the energy convected parallel to the interface (see below). In a series of nine experiments, we find that the Stefan condition accounts for only an average of 52 ± 12 % of the total energy required to evaporate the liquid at the measured rate. Thus, since the buoyancy-driven convection is absent in the experiments we report, thermocapillary convection appears to be an important energy transport mechanism during evaporation, and if thermocapillary convection of water is neglected, conservation of energy would not be satisfied. This also points towards the presence of thermocapillary convection in pure water.

An unexpected observation is the oscillation of the cantilever probe during steady-state evaporation. These oscillations indicate that even at the lowest evaporation rate considered, the flow parallel to the surface is oscillatory, and at higher rates of the evaporation the flow becomes turbulent. This turbulent transition is accompanied by a bifurcation in the relations between the variables that, at lower evaporation rates, was one to one. And the power spectrum of the probe oscillations indicate much stronger oscillations at new characteristic frequencies, but also that continuum of frequencies are present in the flow after the turbulent transition.

Oscillatory flow induced by buoyancy-driven convection during evaporation of liquids other than water have been previously reported [15,16], but we emphasize that the oscillatory flow we report was observed in the absence of any buoyancy-driven convection and our observations are for water. Also, "interfacial turbulence" induced by the absorption of one liquid by another has been previously reported, but Sternling and Scriven point out that the term "turbulence" was used only descriptively at that time. ("Both highly irregular and more or less ordered flows originating in the interface are included in the name" [17].) The general understanding of turbulence is somewhat different now. We choose the term turbulence to describe the flow because (l) the variables bifurcate when the turbulent transition occurs, (2) the magnitude of the flow oscillations are larger in the turbulent flow regime, and (3) the power spectrum indicates

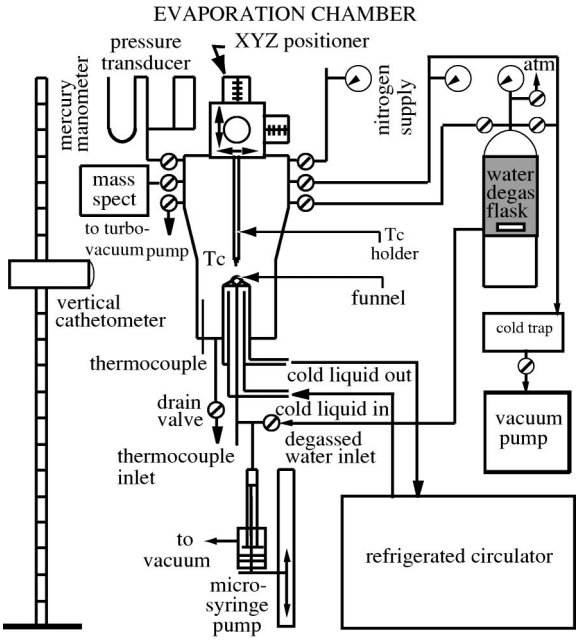

FIG. 2. Evaporation chamber and associated equipment that were used to perform steady-state water evaporation experiments. The funnel indicated in Fig. 1(b) was put at the position indicated.

new dominate oscillations and a continuum of oscillations in the interfacial flow after the turbulent threshold is reached.

II. EXPERIMENTAL METHODS AND RESULTS

The water used was deionized, distilled, nanofiltered, and then transferred into a glass container where it could be degassed before being pumped into the evaporation chamber that is shown schematically in Fig. 2. This preparation procedure gave water with a resistivity of $18.2\times10^6\ \Omega$ cm, and a surface-tension that was within 0.3% of the documented value. Once the water had been degassed, it was transferred (without exposure to air) directly into a glass and Teflon syringe that was mounted in a syringe pump. The pump could push water at a carefully controlled rate through stainless-steel tubing into the bottom of the stainless-steel funnel [Fig. 1(b)] that was mounted in the chamber. Water just outside the mouth of the funnel could be viewed from outside the chamber with a cathetometer and exposed to a reduced pressure.

This chamber with the funnel enclosed was used to run two sets of steady-state evaporation experiments. In the first, a U-shaped (25.4-μm-diameter) thermocouple was mounted on a positioning micrometer that could move the thermocouple in three-dimensions. Two cathetometers were placed so the position of the thermocouple could be measured from outside the chamber. Another thermocouple (enclosed in 0.81-mm-diameter stainless-steel sheath) was permanently placed near the (1.12-mm–diameter) throat of the funnel [Fig. 1(b)]. In each experiment, a water-vapor interface was maintained outside the mouth of the stainless-steel funnel. Its maximum height above the funnel mouth, z_0, was approximately 1 mm in each experiment, and the funnel mouth radius, x_m, was 3.5 mm For these values of z_0, the water-vapor interface may be approximated as spherical. Its area is then $\pi(z_0^2+x_m^2)$.

In the second set of experiments, the U-shaped thermocouple was replaced with a metal cylinder mounted as a cantilever on the positioning micrometer. The cylindrical probe was approximately vertical. Its lower tip could be immersed in the liquid phase by a controlled amount and at a chosen horizontal distance from the center line. During each of the second set of experiments, the position of the probe as a function of time was recorded with a video camera mounted on the telescope of the cathetometer.

A. Experimental procedure

In preparation for an experiment, the evaporation chamber, tubing and syringe were evacuated for 12 h. The chamber reached a pressure of $\sim10^{-5}$ Pa using the turbomolecular and mechanical-backing pump. The gas phase was monitored with a mass spectrometer (SRS® Model RGA 200) both before and after each experiment to ensure no oil vapor from the pumping system entered the evaporation chamber.

After degassed water was introduced into the syringe, the syringe pump was advanced until the liquid-vapor interface had a height of ~1 mm above the mouth of the funnel. To prevent subsequent bubble nucleation, the chamber was then subjected to a period of pressurization. Nitrogen was admitted to the chamber and the pressure maintained at ~42 kPa for a period of 6 h. Afterwards, the water in the tube that had been present in the funnel and in the tubing during the pressurization were flushed out and into the chamber. The chamber was dried by evacuating it with the mechanical vacuum pump.

The syringe pump was advanced to bring the liquid-vapor interface back to a position of z_0 above the mouth of the funnel. Ideally, at this time there would have been only water and its vapor present in the chamber. The conditions in the two sets of experiments are listed in Tables I and II.

With the liquid at the mouth of the funnel, the liquid at the funnel throat was brought to 3.56 ± 0.03 °C and maintained constant at that value. A steady-state evaporation rate was established by adjusting a metering valve that connected the chamber to the vacuum system while the syringe pumping rate was set at a particular value. This process was continued until the position of the liquid-vapor interface did not move by more than ±10 μm during the course of an experiment. When this was achieved the system was judged to be operating in steady-state. Under this condition, the rate at which water was pumped into the bottom of the funnel was equal to the rate at which the evaporation was taking place. The syringe pumping rate could then be measured by determining the change in the syringe plunger position (±10 μm) during the steady-state period. The pressure was measured with a pressure transducer (Omega PX8ll-005GAV) positioned ~19.0 cm above the liquid-vapor interface. The mean evaporation flux measured in each of the experiments is listed in Tables I and II.

B. Temperature and pressure measurements—the control variable

After the liquid was evaporating under steady-state conditions, the temperature in the two phases was measured on

TABLE I. Thermal conditions measured in liquid and vapor-phases during steady-state evaporation.

Experiment:	EV1	EV2	EV3	EV4	EV5	EV6	EV7	EV8	EV9
Vapor phase Press./(Pa)	776.1±12.6	698.8±11.9	599.0±9.9	499.7±8.5	397.9±6.8	299.7±7.1	271.3±5.1	268.4±5.3	247.5±4.5
Intf. Ht. (mm)	1.00±0.01	1.05±0.01	1.01±0.01	0.96±0.01	1.00±0.01	1.01±0.01	1.00±0.01	1.00±0.01	0.99±0.01
Avg. Evap. Flux/ (g/m^2 s)	0.407±0.006	1.002±0.011	1.371±0.015	1.788±0.018	2.544±0.025	3.378±0.031	3.026±0.028	4.242±0.039	3.421±0.032
Throat temp/(°C)	3.52±0.05	3.51±0.05	3.59±0.04	3.56±0.03	3.60±0.04	3.54±0.03	3.59±0.05	3.59±0.10	3.57±0.03
T_I^V/(°C)	4.73±0.02	3.37±0.02	1.84±0.05	−0.20±0.05	−2.65±0.05	−5.66±0.02	−7.19±0.04	−7.59±0.06	−7.31±0.08
T_I^L/(°C)	2.73±0.03	1.11±0.02	0.53±0.03	−2.82±0.03	−6.04±0.03	−9.67±0.03	−11.61±0.03	−12.06±0.04	−11.86±0.03
Unif.-Temp. Layer[a]/ (mm)	0.35±0.01	0.17±0.01	0.13±0.01	0.09±0.01	0.07±0.01	0.07±0.01	0.05±0.01	0.05±0.01	0.05±0.01
Tangential Speed (mm/s)	0.126±0.000	0.433±0.005	0.417±0.001	0.615±0.004	0.549±0.005	0.534±0.001	1.123±0.004	0.722±0.014	0.934±0.002

[a]On the center line.

the funnel center line and in one horizontal direction at horizontal distances of 0.7, 1.4, 2.1, and 2.8 mm from the center line, and at different vertical positions at each horizontal position. At each position, the temperature was recorded every second for a period of approximately 1 min (by a Labview program and a Hewlett Packard Data Acquisition/Switch Unit, 34970A). The mean and standard deviation were then calculated. The interfacial values on the center line are listed in Table I.

Once the temperature had been measured in one horizontal direction and without opening the system or changing the experimental conditions, the thermocouple positioner was rotated 90° and the temperature measured in a second horizontal direction. In this case also, the temperature was measured on the center line and at horizontal distances of 0.7, 1.4, 2.1, and 2.8 mm from it and at different vertical positions. When the temperature was measured at a position, the pressure was also measured, using a pressure transducer (Omega PX811-005GAV). All of the pressures measured during an experiment were averaged to establish the mean (±SDV, Table I).

In each experiment of both sets, the pressure in the vapor-phase, P^V, the evaporation rate, J_{ev}, and the temperature of the water at the funnel throat, T_{th}, were measured. The mean evaporation flux, $\overline{j_{ev}}$ was calculated from the directly measured J_{ev} and the area of the liquid-vapor interface. In the second set of experiments, the values of T_{th}, P^V, z_0, and $\overline{j_{ev}}$ were chosen to have approximately the same values as one of the experiments conducted when the temperature field was measured. The measured values of these variables are listed in Tables I and II.

TABLE II. Thermal conditions existing when the thermocapillary speed was measured.

Experiment:	EV10	EV11	EV12	EV13	EV14	EV15
Vapor-phase pressure (Pa)	820.1±12.5	599.1±11.2	500.3±8.2	399.4±6.8	299.7±5.1	274.3±4.2
Max. interface height/(mm)	1.00±0.01	1.01±0.01	1.00±0.01	1.00±0.01	1.00±0.01	1.00±0.01
Evaporation flux (g/m^2 s)	~0	1.466±0.011	2.002±0.014	2.669±0.018	3.403±0.023	3.537±0.024
Throat temperature TC3 (°C)	3.55±0.04	3.57±0.03	3.58±0.04	3.58±0.05	3.54±0.05	3.54±0.05
Probe position (x_p/x_m)	0.485	0.468	0.463	0.469	0.460	0.451
Mean probe deflection, $\overline{y_{\mathrm{Max}}}$/pixels	0	2.02±0.68	1.97±0.94	2.00±1.20	1.70±0.91	2.60±1.40
Probe amplitude/(pixels)	0	3±1	3±1	4±1	4±1	6±1
Tangential speed (mm/s)	0	0.63±0.20	0.57±0.26	0.53±0.30	0.40±0.20	0.57±0.28

Probe modulus of elasticity: 141.13±0.79 GN/m^2 and density 8.73×10^3 kg/m^3

Probe length, L: 52 mm

Probe diameter: D_p: 12.7 μm

Probe immersion depth: I_d: 40 μm

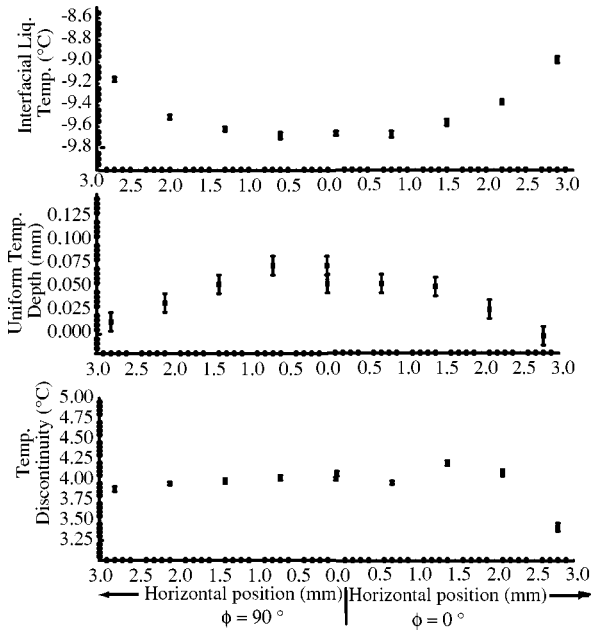

FIG. 3. The abscissa indicates the position measured from the center line in each of two horizontal directions separated by 90°. The upper ordinate gives the interfacial liquid temperature. The middle ordinate gives the thickness of the uniform-temperature layer and the lower ordinate gives the interfacial temperature discontinuity. For this experiment, water was evaporating at a steady rate of 3.378 ± 0.031 g/m^2 s, and the pressure in the vapor phase was 299.7 ± 7.1 Pa.

As P^V was reduced from 776 Pa (EV 1) to 300 Pa (EV 6), the interfacial temperature became progressively more parabolic. In each case, the minimum interfacial temperature occurred on the center line and the maximum at the periphery. For the latter experiment, the measured conditions near the interface are shown in Fig. 3. The depth of the uniform-temperature layer was a maximum on the center line, and the interfacial temperature discontinuity was approximately uniform at 4 °C. Thus, the interfacial vapor temperature was approximately parallel to that of the liquid, but ~4 °C above it.

The temperature measured as a function of depth in the experiment conducted at 300 Pa (EV 6) is shown in Fig. 4. Note the "uniform" temperature layer. To a depth of ~0.1 mm, there was no statistical difference between the measured temperatures. The temperature profile below the uniform-temperature layer was again observed to have a constant gradient [8]. Thus, thermal energy was being conducted to the uniform-temperature layer, but the mechanism by which it crossed the uniform-temperature layer was not thermal conduction. The dashed line was simply drawn through the mean values of the temperature measurements. The error bars were calculated from the standard deviation of the measured temperature and are not visible on this scale.

The temperature at the throat in this experiment was 3.54 ± 0.03 and −9.67 °C at the interface on the center line. Thus, the liquid temperature was below 4 °C and decreased with height. Since the density decreases with temperature in this temperature range, there would not have been any buoyancy-driven convection. The experimental conditions in each of our experiments were similar to those indicated in Fig. 4. Thus, buoyancy driven convection was absent in each of them.

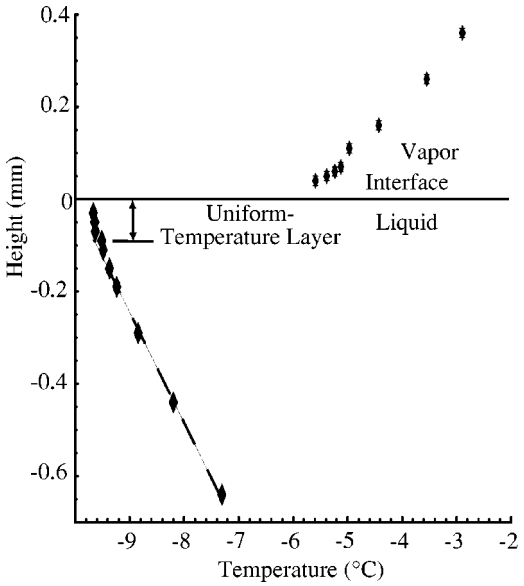

FIG. 4. Measured temperature profile on the center line in the liquid and vapor-phases when water was evaporating with an average flux of 3.378 ± 0.031 g/m^2 s. The vapor-phase pressure was approximately 300 Pa.

Similar interfacial liquid temperature profiles were observed when the pressure was reduced below 300 Pa. But as indicated in Fig. 5, at these lower pressures P^V no longer acts as the control variable for $\dot{j}_{ev}$. For P^V greater than 300 Pa, there is a one-to-one relation between $\dot{j}_{ev}$ and P^V, but for smaller values of P^V, more than one value of P^V is indicated

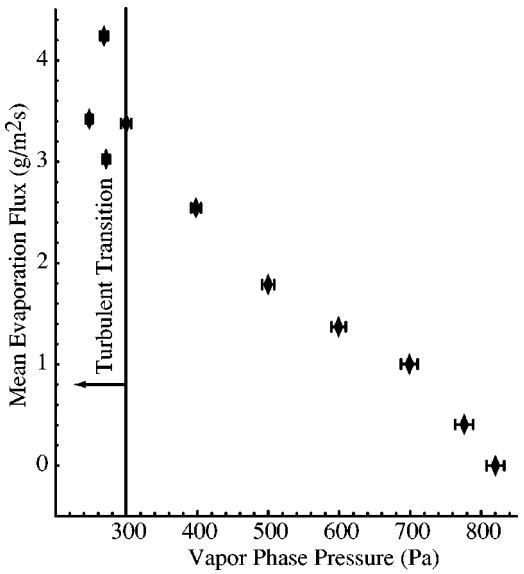

FIG. 5. The evaporation flux measured as a function of the vapor-phase pressure during steady-state water evaporation. Note that for pressures below 300 Pa, the vapor-phase pressure no longer acts as the control variable.

to give the same value of $\overline{j_{ev}}$. We emphasize that in all experiments the temperature at the funnel throat was maintained at 3.56 ± 0.03 °C. The bifurcations in the other experimental variables are discussed in subsequent sections.

C. Tangential fluid speed from the surface-tension gradient

When there is a gradient in the interfacial liquid temperature, such as that found in these experiments (see Fig. 3), the Marangoni effect would be expected to give rise to convective flow from the periphery toward the center line. To calculate the magnitude of the fluid speed parallel to the liquid-vapor interface, we suppose the liquid phase may be approximated as incompressible, its shape as spherical with radius R_0 and as having axisymmetric properties.

The interfacial radius is given by

$$R_0 = \frac{x_m^2 + z_0^2}{2z_0}.$$

If the motion of the fluid is approximated as quasisteady, the shear stress in spherical coordinates (r, θ, ϕ) at the interface in the i_θ direction, $\sigma_{r\theta}(R_0, \theta)$ would be balanced by the gradient in the surface-tension, γ^{LV} which we assume to depend only on temperature:

$$\nabla \gamma^{LV} \cdot i_\theta = \frac{1}{R_0}\left(\frac{d\gamma^{LV}}{dT_I^L}\right)\frac{dT_I^L}{d\theta}. \tag{1}$$

The shear stress at the interface of the axisymmetric liquid phase may be expressed in terms of the angular and radial components of the velocity, v_θ and v_r and the viscosity, η [18]:

$$\sigma_{r\theta}(R_0, \theta) = \eta \left(\frac{1}{r}\frac{\partial v_r}{\partial \theta} + \frac{\partial v_\theta}{\partial r} - \frac{v_\theta}{r}\right)\Bigg|_{r=R_0}. \tag{2}$$

We shall neglect the variation of v_r with θ, and define the variable x as

$$x \equiv \ln\left(\frac{r}{R_0}\right). \tag{3}$$

then Eq. (2) may be written

$$\sigma_{r\theta}(R_0, \theta) = \eta\left[\frac{\partial}{\partial x}\left(\frac{v_\theta}{r}\right)\right]_{x=0}. \tag{4}$$

After equating Eqs. (4) and (1), one finds

$$\left[\frac{\partial}{\partial x}\left(\frac{v_\theta}{r}\right)\right]_{x=0} = \frac{1}{\eta R_0}\left(\frac{d\gamma^{LV}}{dT_I^L}\right)\left(\frac{dT_I^L}{d\theta}\right). \tag{5}$$

A series expansion may be used to obtain an expression for v_θ/r at a radial position near the interface, $R_0 - l \leqslant r \leqslant R_0$. We take the value of l to be where v_θ vanishes. When r has the value $(R_0 - l)$, x would have the value. $\ln(1 - l/R_0)$. If only the first two terms in the expansion are retained:

$$\left[\frac{v_\theta}{r}\right]_{x=\ln(1-l/R_0)} = \left[\frac{v_\theta}{r}\right]_{x=0} + \left[\frac{\partial}{\partial x}\left(\frac{v_\theta}{r}\right)\right]_{x=0}[\ln(1 - l/R_0)]. \tag{6}$$

By definition of l, the left-hand side of the Eq. (6) vanishes.

To estimate the value of l the nature of the flow in the unstirred layer may be considered. The measured temperature profiles indicate that in each experiment the thermocapillary flow at the interface will be directed toward the center line. At some depth, the conservation of mass principle would require the angular speed to be in the opposite direction. Between these two positions, v_θ must vanish. If the thickness of the uniform-temperature layer is denoted as δ_u and this layer is assumed to be generated by the interaction between the oppositely directed streams, then the position where v_θ vanishes would be approximately at the depth of the uniform-temperature layer; thus, we shall assume l is equal δ_u. From Eqs. (5) and (6), the speed at the interface is given by

$$v_\theta(R_0, \theta) = -\frac{1}{\eta}\left(\frac{d\gamma^{LV}}{dT_I^L}\right)\left(\frac{dT_I^L}{d\theta}\right)[\ln(1 - \delta_u/R_0)]. \tag{7}$$

The dependence of T_I^L on θ may be determined from the experimental data by assuming

$$T_I^L = a_T + b_T \sin^2 \theta, \tag{8}$$

and evaluating the coefficients (a_T, b_T) from the measurements made in each experiment.

Also, the same approach may be used to determine an analytical expression for the thickness of the uniform-temperature layer. The value of δ_u as a function of θ was determined from curves such as that shown in Fig. 4. These curves were obtained at each of the nine horizontal positions where the temperature was measured as a function of height. If it is assumed that δ_u is of the form,

$$\delta_u = c_0 + c_1 \sin^2 \theta + c_2 \sin^4 \theta, \tag{9}$$

then, for each experiment, the values of $c_j (j = 0, 1, 2)$ may be determined from measured values of δ_u. When the empirically determined coefficient values are used in Eqs. (8) and (9), the value of the angular speed may be calculated. To examine the magnitude of the speed, the calculated values of v_θ at the mid-point between the center line and the wall for each experiment of the first set (Table) I are shown in Fig. 6 as a function of P^V. Note that the tangential speed at the interface varies significantly with P^V, reaching a maximum of ~1 mm/s.

D. Probe measurement of the fluid speed

The values of v_θ calculated from Eqs. (7)–(9) rely on the measurements of the temperature profile and the thickness of the uniform-temperature layer. A second method for determining the fluid speed is to use the measured deflection of the probe and the elastic properties of the probe material. In the second set of experiments, the same procedure was used to establish a water-vapor interface at the mouth of the funnel. The probe, attached as a cantilever on the positioning

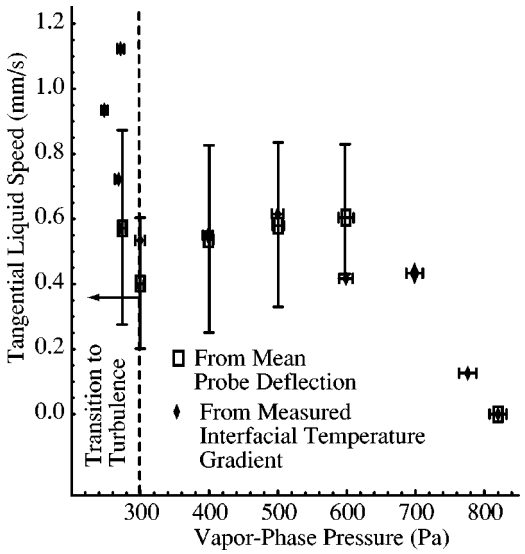

FIG. 6. Summary of the values of the liquid speed tangential to the surface determined by two techniques during water evaporation under steady-state conditions. Note the sudden change in the speed when the vapor-phase pressure is reduced below 300 Pa.

micrometer, was immersed into the uniform-temperature layer at a depth of 40 μm.

The force on the cantilever tip, F_c, required to produce a defection there of $y_{\max}$ when the cantilever is of length L, has a modulus of elasticity E and a diameter D_p may be expressed as

$$F_c = \frac{3\pi E D_P^4 y_{\max}}{64 L^3}. \tag{10}$$

In the Oseen approximation, the low Reynolds number flow of an incompressible fluid perpendicular to a cylinder of diameter D_p, and of infinite length produces a drag per unit length [19], F_{drag} of

$$F_{\text{drag}} = \frac{4\pi\eta v_\theta}{0.077 + \ln\left(\frac{\rho^L v_\theta D_p}{8\eta}\right)}. \tag{11}$$

If the probe is immersed to a depth of I_d, then the total force would be the product of this depth and F_{drag}. Since I_d is small compared to the cantilever length (52 mm), we approximate the drag force as being applied at the end of the cantilever. After multiplying Eq. (11) by I_d and equating the result to Eq. (10), one finds an equation that relates the fluid speed v_θ to the probe-tip deflection $y_{\max}$:

$$v_\theta - \frac{3EI_d y_{\max}}{4\pi\eta I_d L^3}\ln\left[\frac{\rho^L D_p v_\theta}{8\eta}\right] = \frac{0.231 E D_p^4 y_{\max}}{256\eta I_d L^3}. \tag{12}$$

In Eq. (12), we take the value of $y_{\max}$ be that resulting from the mean tangential flow. There is also a fluctuating component of the flow (as will be seen), but the measured temperature gradient along the surface is the steady-state gradient, since its value is based on the time-average values of the temperatures; thus, the flow corresponding to the measured gradient would be the mean flow.

To determine the probe deflection, the image of the probe was recorded just before the probe was immersed, and the position of the probe tip relative to a position 160 μm (31 pixels) above the probe tip was determined. After the probe tip was immersed, the position of the probe was recorded every 0.5 s for a period of 30 s using a video camera mounted on a telescope, and the images were analyzed (NIH Image 1.61/68 K and a Apple^{TM} Quadra, 840 AV). From each image, the position of the probe tip was determined at each time relative to the position 160 μm above the tip. The change in the relative position of the probe tip following its immersion is taken to be the value of y_{Max} at each of the these 60 times. From these values, the mean, $\overline{y_{\text{Max}}}$ and the standard deviation for each experiment were calculated. Their values are listed in Table II. Only the value of $\overline{y_{\text{Max}}}$ is used in the calculation of v_θ, but note that the fluctuations about the mean are significant. The fluctuations are discussed in Sec. III.

The tangential fluid speed calculated from $\overline{y_{\text{Max}}}$ using Eq. (12) for each experiment in the second set is shown in Fig. 6 where they may be compared with the speed calculated from the surface-tension gradient using Eqs. (7)–(9). Since the probe was immersed into the liquid phase only 40 μm the probe would have only experienced the conditions in the uniform-temperature layer. Thus, the values of v_θ calculated from it should correspond with the surface speed. Note that the calculated mean speed obtained from the probe measurements coincides with the value of the speeds determined from the surface-tension measurements in two of the five experiments, and the mean error in the five experiments was 18%. This agreement between the tangential speeds, calculated from the surface-tension gradient and determined from the drag on the probe, strongly supports the existence of thermocapillary convection for pure water.

E. Transition to turbulence in the uniform-temperature layer

The potential for inducing fluid flow tangential to the interface by the Marangoni effect is the difference in the temperature between the periphery and the center line, denoted as ΔT_{R0}:

$$\Delta T_{R0} \equiv [T_I^L(2.8\text{ mm}) - T_I^L(0)].$$

Two flow regimes within the uniform-temperature layer may be identified on the basis of ΔT_{R0} values. As seen in Fig. 7, for values of ΔT_{R0} less than 0.6° C, there is a one-to-one relation between ΔT_{R0} and $\overline{j_{ev}}$ The value of ΔT_{R0} is equal to 0.6 °C when P^V is 300 Pa, and becomes greater than 0.6 °C when P^V is reduced below 300 Pa. Hence for $\Delta T_{R0} < 0.6$ (or P^V greater than 300 Pa), ΔT_{R0} and $\overline{j_{ev}}$ have a one-to-one relation. Also, in this P^V range, $\overline{j_{ev}}$ (Fig. 5) and v_θ (Fig. 6) each bear a one-to-one relation to P^V. Thus, the flow within the uniform-temperature layer is possibly laminar for this limited pressure range.

In Fig. 8, the measured amplitude of the probe oscillations as a function of time is shown. In experiment EV 10, there was no measurable evaporation rate, and there were no mea-

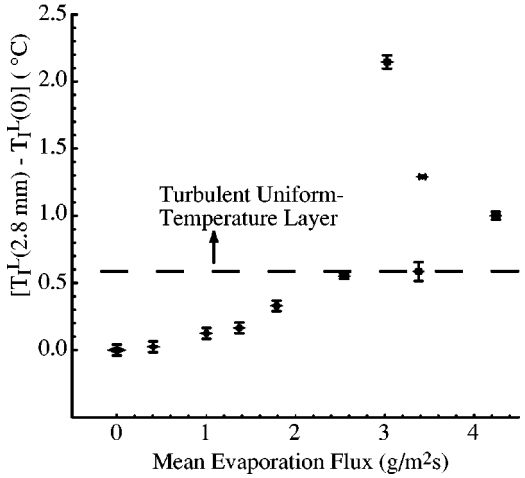

FIG. 7. Relation between the mean evaporation flux and the temperature difference between the periphery and the center line. Note the sudden change in the relation when the temperature difference is greater than 0.6 °C. This value of the temperature difference is reached when the pressure is reduced below 300 Pa.

surable oscillations of the probe. In EV 11, $\underline{P^V}$ was reduced to 600 Pa and the measured value of $\underline{j_{ev}}$ increased to 1.466 g/m^2 s. The mean displacement (±SDV) of the probe toward the center line was 2.02±0.68 pixels (Table II). It oscillated with a amplitude of ±1 pixel. Thus, it appears that

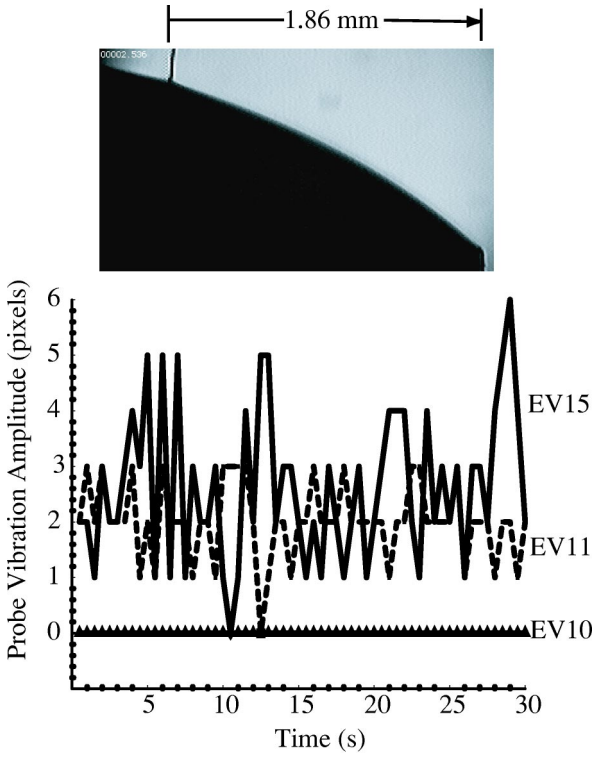

FIG. 8. An image of the 12.7-μm-diameter metal probe immersed in the liquid phase during experiment EV 11 is shown in the upper illustration. The immersed probe underwent oscillations that depended on the rate of evaporation, lower illustration. The experimental conditions existing during experiments EV10, EV11, and EV 15 are listed in Tables I and II.

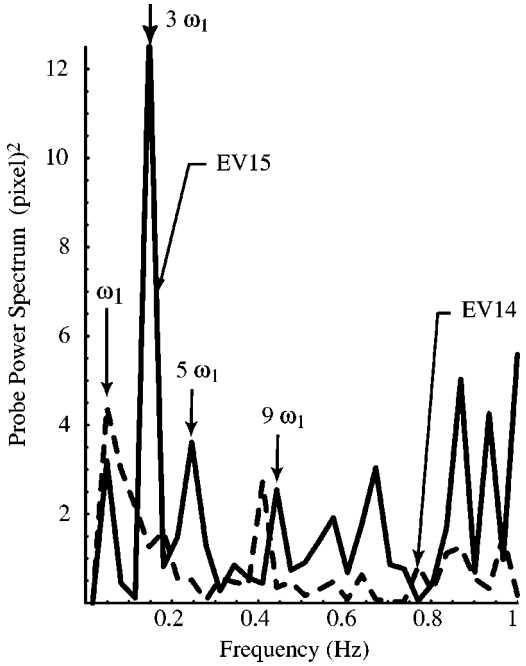

FIG. 9. Spectrum of the probe oscillations. The probe oscillation amplitude was sampled at 2 Hz. The vapor-phase pressure during EV 14 was 297.7±5.1 Pa, but in experiment EV15 the pressure was reduced to 274.3±4.2 Pa (Tables I and II).

even at the smallest evaporation rate considered, the flow within the uniform-temperature layer is not laminar but oscillatory.

When $\Delta T_{R0} \geqslant 0.6$ (or $P^V \leqslant 300$ Pa), there are a number of relationship changes. There is no longer a one-to-one relation between P^V and $\underline{j_{ev}}$ (Fig. 5). Neither is there one between the mean tangential speed, v_θ and P^V (Fig. 6), nor between $\underline{j_{ev}}$ and ΔT_{R0} (Fig. 7). In each case, the relationship between the variables could be described as undergoing a bifurcation in the sense that what was a one-to-one relation between the variables became a one-to-two relation. Note that for a given P^V, there is more than one value of v_θ (Fig. 6). Since v_θ is not controllable by the macroscopic variables in this range of parameters, the fluid motion is at least chaotic and possibly turbulent. However, the bifurcations are not shear induced. The Reynolds number is of order unity.

The power spectra of the probe oscillations for experiments EV 14 and EV 15 are shown in Fig. 9. The spectrum of EV 14 indicates oscillatory flow with the principal frequency at 0.05 Hz, denoted as ω_1. However, there was limited energy associated with this frequency when P^V was 300 Pa or ΔT_{R0} was 0.6 °C and frequency oscillations were damped out. The experiments conducted at higher pressures (EV 11 through EV 13) also indicated oscillations were present, but did not share this frequency.

When P^V was reduced by 274.3 Pa, there was a dramatic change in the spectrum (see Fig. 9). The power spectrum of EV 15 indicates that the basic frequency at 0.05 Hz was again present, along with a new and dominant frequency at $3\omega_1$ and a third and fourth frequency at $5\omega_1$ and $9\omega_1$. Such a power spectrum corresponds to the probe displacement being a periodic function with frequency locking [20]. (We limit

our attention to the portion of the spectrum less than 0.25 times the sampling frequency.) Thus, in this case, the fluid motion was such that higher frequencies were not damped out. Their presence indicates that the fluid motion was turbulent and not just chaotic.

The natural frequency of the cantilevered probe, ω_N may be estimated by equating the force on the probe tip [Eq. (10)] to the product of the probe mass $\pi D_p^2 L \rho_p/4$ with its acceleration $y_{\max}\omega_N^2$. One then finds

$$\omega_N = \frac{1}{2\pi}\left(\frac{3D_P^2 E}{16L^4\rho_p}\right)^{1/2}. \tag{13}$$

After inserting the values of D_p, L, ρ_p, and E that are listed with Table II, one finds

$$\omega_N = 1.3 \text{ Hz}. \tag{14}$$

This frequency is more than 25 times greater than the frequency ω_1 that appears with its harmonics in the spectra, and ω_N is well outside the frequencies indicated to be characteristic of the flow (see Fig. 9). Thus, ω_1 and its harmonics appear to characteristic of the flow generated by water evaporation.

III. DISCUSSION AND CONCLUSION

The mechanism by which the uniform-temperature layer is produced immediately below the liquid-vapor interface appears to be the mixing resulting from the thermocapillary flow in this layer (see Fig. 4). The fluid speed tangential to the liquid-vapor interface was measured at only one point in the uniform-temperature layer, but the temperature profile suggests there would have been flow all along the liquid-vapor interface directed from the periphery toward the center line. At the center line, the mixing would have been the most intense, and it was at this position that the thickness of the uniform-temperature layer was the greatest (see Fig. 3). The average fluid speed perpendicular to the liquid-vapor interface, i.e., the average flow required by the evaporation was small compared to the thermocapillary flow. For example, in experiment EV 14 the average speed perpendicular to the liquid-vapor interface averaged 3.4 μm/s but the flow rate tangential to the liquid-vapor interface was 400 μm/s (Table II). Thus, there would have been a return-flow below the interface from the center line toward the periphery. The interaction between the thermocapillary and the return-flow would have given rise to mixing.

The examination of the probe motion indicates that even at the lowest evaporation rate examined (1.466 g/m^2 s), the thermocapillary flow was oscillatory (see Fig. 8). As P^V was lowered, the speed of the thermocapillary flow increased (see Fig. 6), but the uniform-temperature layer became thinner, forcing a stronger interaction between the two streams, possibly giving rise to the growing oscillations in the flow and to the transition to turbulence.

These measurements give a physical explanation for the uniform-temperature layer, but the presence of the uniform-temperature layer raises questions regarding the analytical procedures that can be used to predict the temperature and

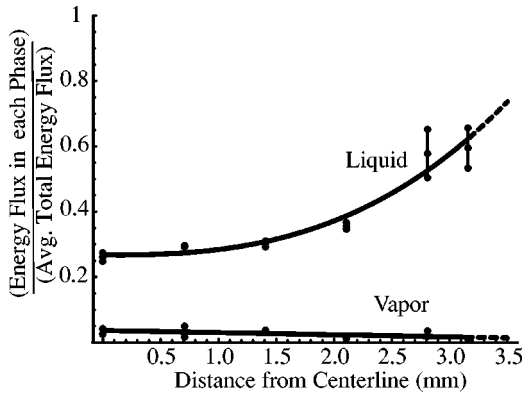

FIG. 10. Energy flux through each bulk phase as a fraction of the total, average energy flux required to evaporate the liquid at the measured rate.

velocity fields near the interface. One of the basic questions raised is that regarding the Stefan condition [13,14]. The basis for this relation is conservation of energy. For example, if one considers an element of volume, such as that shown in Fig. 1(a) that encloses a portion of both the liquid and vapor phases, then provided the kinetic energy and viscous dissipation within the layer are negligible, conservation of energy requires

$$\oint_{A_L}(\rho_L h_L v_L - \kappa_L \nabla T_L)\cdot dA_L + \oint_{A_V}(-\rho_V h_V v_V - \kappa_V \nabla T_V)\cdot dA_V = \left(\frac{d}{dt}\right)\left(\int_{V_L}\rho_L u_L dV_L + \int_{V_V}\rho_V u_V dV_V\right), \tag{15}$$

where enthalpy, internal energy, fluid velocity and the thermal conductivity are denoted as h, u, v, and κ, and a subscript L or V refers a property to the liquid or vapor phases. The area of the enclosing surface is denoted as A_i and the volume as V_i. If a limit of this equation is taken in which the extent of the volume element normal to the surface is reduced to zero, Eq. (15) reduces to the conventional Stefan condition [13,14]

$$-\kappa_L\left(\frac{\partial T_L}{\partial n_L}\right)_I - \kappa_V\left(\frac{\partial T_V}{\partial n_V}\right)_I = j_{ev}(h_V - h_L), \tag{16}$$

where j_{ev} is the net evaporation flux.

Both $(\partial T_L/\partial n_L)$ and $(\partial T_V/\partial n_V)$ can be measured directly (see Fig. 4) at each position where the temperature profile in a bulk phase was measured and the values of the thermal conductivities calculated at the interfacial position [21]; thus, the validity of the Stefan condition can be examined. The type of results obtained are shown in Fig. 10 which indicates the energy flux through each bulk phase perpendicular to the interface. This flux was calculated at a point from the measured temperature profiles at that point during experiment EV 8 (see Table I). Strictly speaking, the energy flux through the liquid phase evaluated at the interface would be zero since $(\partial T_L/\partial n_L)_I$ vanishes there. The values shown for the liquid phase were calculated from the temperature profile measured at the bottom of the uniform-temperature layer. In

Fig. 10, the energy flux at a point through each bulk phase is expressed as a fraction of the average, total energy flux required to evaporate the liquid, $\overline{q_{ev}}$ at the measured rate. The enthalpy difference was determined from the tabulated value, $h_{fg}(T_{3p})$ available at the triple point of water, T_{3p}:

$$h^V - h^L = h_{fg}(T_{3p}) + c_p^V(T^V - T_{3p}) - c_p^L(T^L - T_{3p}). \quad (17)$$

One finds the value of $(h^V - h^L)$ varies by less than 1% along the liquid surface. Thus, the average total heat flux required to evaporate the liquid is approximately given by

$$\overline{q_{ev}} = (h^V - h^L)J_{ev}/A_{LV}, \quad (18)$$

where A_{LV} is given by $\pi(z_0^2 + x_m^2)$. Recall that J_{ev} and z_0 were directly measured in each experiment (Table I).

The error bars shown in Fig. 10 indicate the difference in the heat flux obtained from two temperature traverses that were measured along the interface in two directions separated by 90°. If the temperature field were perfectly axisymmetric and the measurement perfectly repeatable, the error bars would have been reduced to zero. In this experiment, measurements were made on the centerline, and 0.7, 1.4, 2.1, 2.8, and 3.15 mm from it. The extrapolation, shown as a dashed line in Fig. 10, was 0.35 mm in length. Note that at no point do the fractional energy fluxes through the bulk phases add up to be unity, as they would do if the energy conducted through the liquid and vapor phases were sufficient to evaporate the liquid at the measured rate. In this particular experiment (EV 8), the sum varies from ~0.3 on the center line to ~0.8 at the periphery (Fig. 10).

By numerically integrating the results shown in Fig. 10, one can calculate the total energy transport rate to the interface for this experiment, EV 8. One finds that less than 50% of the energy required to evaporate the liquid at the measured rate is conducted to the interface through the bulk phases. The remainder must be convected by the thermocapillary flow from the funnel wall. Following a similar procedure, for the other eight experiments described in Table I, one can determine the fraction of the energy transported to the interface by conduction. One finds that on average only $52 \pm 12\%$ of the energy transport rate comes from the conduction through the bulk phases. Thus, the energy transport by thermocapillary convection appears to play a major role in transporting the energy required to evaporate the liquid.

ACKNOWLEDGMENTS

The authors gratefully acknowledge many helpful suggestions from Professor K. Danov and Professor F. Durst, Friedrich-Alexander-Universitat, Erlangen-Nurnberg, Germany and thank the Canadian Space Agency and the Natural Sciences and Engineering Research Council of Canada for financial support.

[1] A-T. Chai and N. Zhang, Exp. Heat Transfer **11**, 187 (1998).
[2] G. T. Barnes and D. S. Hunter, J. Colloid Interface Sci. **88**, 437 (1982).
[3] J. R. A. Pearson, J. Fluid Mech. **4**, 489 (1958).
[4] H. J. Palmer, J. Fluid Mech. **75**, 487 (1976).
[5] H. K. Cammenga, D. Schreiber, G. T. Barnes, and D. S. Hunter, J. Colloid Interface Sci. **98**, 585 (1984).
[6] Y. Garrabos, C. Lecontre-Chabot, J. Hegseth, V. S. Nikolayev, D. Beysens, and J.-P. Deville, Phys. Rev. E **64**, 051602 (2001).
[7] S. Terakado, F. Takemura ,Y. Yabe, S. Terakado, F. Takemura, and A. Yabe, Proceedings of the National Heat Transfer Conference Paper No. NHT200I-20142, 2001.
[8] C. A. Ward and G. Fang, Phys. Rev. E **59**, 429 (1999).
[9] G. Fang and C. A. Ward, Phys. Rev. E **59**, 417 (1999)
[10] G. Fang and C. A. Ward, Phys. Rev. E **59**, 441 (1999).
[11] A. J. H. McGaughey and C. A. Ward, J. Appl. Phys. **91**, 6406 (2002).
[12] C. A. Ward and D. Stanga, Phys. Rev. E **64**, 051509 (2001).
[13] L. E. Sissom and D. R. Pitt, *Elements of Transport Phenomena* (McGraw-Hill, Toronto, 1972), p. 655.
[14] J. Stefan, Ann. Phys. Chem. **42**, 269 (1891).
[15] N. Zhang and W-J. Yang, Trans. ASME, J. Appl. Mech. **104**, 656 (1982).
[16] J. J. Hegseth, N. Rashidnia, and A. Chai, Phys. Rev. E **54**, 1640 (1996).
[17] C. V. Sternling and L. E. Scriven, AIChE J. **5**, 514 (1959).
[18] L. D. Landau and E. M. Lifschitz, *Fluid Mechanics* (Pergamon, London, 1959), p. 52.
[19] L. D. Landau and E. M. Lifschitz, *Fluid Mechanics* (Ref. [18]), p. 68.
[20] P. Berge, Y. Pomeau, and C. Vidal, *Order within Chaos* (Wiley-Interscience, New York, 1986), p. 58.
[21] J. V. Sengers and J. T. R. Watson, J. Phys. Chem. Ref. Data **15**, 1291 (1986).